

Modelling groundwater rebound in recently abandoned coalfields using DInSAR

David Gee ^{a, b*}, Luke Bateson ^c, Stephen Grebby ^a, Alessandro Novellino ^c, Andrew Sowter ^b,
Lee Wyatt ^d, Stuart Marsh ^a, Roy Morgenstern ^e, Ahmed Athab ^b.

^a Nottingham Geospatial Institute, University of Nottingham, Nottingham NG7 2TU, UK

^b Terra Motion Limited, Ingenuity Centre, Nottingham NG7 2TU, UK

^c British Geological Survey, Natural Environment Research Council, Keyworth NG12 5GG,
UK

^d Coal Authority, 200 Lichfield Lane, Mansfield, Nottinghamshire NG18 4RG, UK

^e Geotechnical Institute, TU Bergakademie Freiberg, Saxony 09599, Germany

* Corresponding author: david.gee@nottingham.ac.uk

Abstract

Advances in differential interferometric synthetic aperture radar (DInSAR) processing algorithms, such as the Intermittent Small Baseline Subset (ISBAS), and increased data availability from SAR systems, such as Sentinel-1, provide the opportunity to increase the spatial and temporal density of ground deformation measurements. Such measurements,

when combined with modelling, have the potential to make a significant cost-effective contribution to the progressive abandonment strategy of recently closed coalfields.

Applications of DInSAR over coalfields have observed heave in coal measures rocks and temporal correlations between the rise of mine water and deformation time-series. The cessation of systematic dewatering can have a variety of detrimental impacts and knowledge of the time-scales (i.e. the rate of rebound) and structure of the mine system are crucial to the remediation strategy. Although mine plans and borehole measurements provide vital information in this regard, mine plans are often incomplete or inaccurate, whereas monitoring boreholes are spatially sparse. Consequently, groundwater can flow in unanticipated directions via goaf, mine shafts and roadways, making it difficult to determine where the impacts of rebound are likely to occur. In this study, ground deformation data obtained using ISBAS DInSAR on ENVISAT (2002 – 2009) and Sentinel-1 (2015 – 2019) data are used to develop a simple method to model groundwater rebound in abandoned coalfields. A forward analytical model based upon the principle of effective stress and mine water ponds is first implemented to estimate surface heave in response to changes in groundwater levels measured in monitoring boreholes. The forward model is then calibrated and validated using the ground deformation data. The DInSAR data were subsequently inverted to map the change in groundwater levels in greater detail across the coalfield and forecast surface discharges in order to support mitigation strategies.

Keywords:

Surface Deformation; DInSAR; Intermittent SBAS; Groundwater Modelling; Coal Mining; Dewatering; Heave; Hydrogeology

1. Introduction

Deep underground coal mining almost always extends below the natural water table (Younger, 2016). Accordingly, extensive dewatering of coal measures rocks is required to ensure dry and safe working conditions in collieries, with strategic pumping stations located around the complex network of mine workings (Dumpleton *et al.*, 2001). After colliery closure, the cessation of dewatering results in the progressive rise of groundwater and flooding of old workings and surrounding rock, as the rock matrix begins to revert back to saturated conditions. Acid mine water drainage (AMD) is water that becomes polluted through contact with former workings. AMD can have many adverse consequences, which are listed in order of environmental significance and frequency (Younger & Adams, 1999):

- (i) surface water pollution;
- (ii) localised flooding of agricultural, industrial or residential areas;
- (iii) loss of dilution for other pollutants in surface waters where former pumped discharges have ceased;
- (iv) overloading and clogging of drains and sewers;
- (v) pollution of overlying aquifers by upward movement of mine water (principally from sulphate and chloride);
- (vi) temporarily increased emissions of mine gases, driven ahead of rising mine water;
- (vii) ground deformation due to renewed mining subsidence and reactivation of faults (Donnelly, 2006);
- (viii) adverse effects on landfills – possible damage to lining, leakage of leachate and increased gas emissions.

Methods to estimate the spatial extent and timescales (i.e. the rate of rebound) of mine water rise are vital to generate rational policies and a cost-benefit remediation strategy for progressive mine abandonment (Younger & Adams, 1999; Younger, 2016). Mine plans provide crucial information in the prediction of the directional and structural control of groundwater flow. When above the water table, groundwater flows down-dip through permeable stratigraphic horizons, such as the fractured or jointed sandstones, goaf, collapsed strata and mining roadways. Down-dip flow will stop and groundwater will pond once it reaches a hydraulic barrier such as an intact coal pillar or fault. Water levels will rise until a new overflow point is reached in the form of a drainage adit at the surface or a connection to a neighbouring colliery. However, the prediction of flow is often challenging due to incomplete and inaccurate information regarding inter-seam connections within collieries, as well as connections between adjacent collieries from mine plans that might have been drawn more than a century ago. Flow can therefore occur in unanticipated directions which can lead to surface discharges and pollution in areas not thought to be vulnerable (Younger & Adams, 1999). In addition, monitoring boreholes are expensive and often spatially sparse, providing only a limited overview of mine water levels in complex and often vast mine systems.

Many studies have recognised the impact of changing groundwater levels on the compaction of strata and deformation at the surface (e.g. Hoffman *et al.*, 2001; Galloway & Hoffmann, 2007; Bell *et al.*, 2008, Chaussard *et al.*, 2017, Motagh *et al.*, 2017). As groundwater levels change, compaction or expansion of the subsurface strata occurs due to a change in hydrostatic pressure (Bekendam & Pöttgens, 1995). Conventional monitoring methods for

mapping surface deformation, such as precise levelling, close range photogrammetry and GPS, can be laborious, expensive and offer limited spatial coverage. Remote differential interferometric synthetic aperture radar (DInSAR) is a cost-effective wide-area method to measure sub-centimetre rates of surface deformation. In particular, the emergence of time-series methods in the late 1990s has increased the integration of surface deformation measurements into hydrogeological studies. DInSAR data facilitate the identification of areas of groundwater depletion or recharge, and so provide the means to calibrate groundwater models, delineate lithological boundaries and map aquifer storage variations and assist characterisation (e.g. Chaussard *et al.*, 2014; Castellazzi *et al.*, 2016; Bejar-Pizarro *et al.*, 2017; Castellazzi *et al.*, 2018). Additionally, DInSAR measurements have previously been utilized to calibrate and/or validate models of surface deformation associated with anthropogenic fluid injection or extraction (e.g. Rutqvist *et al.*, 2010; Pearse *et al.*, 2014; Gee *et al.*, 2016). Initial applications over mining areas also confirmed the capability of DInSAR to measure mining induced subsidence (e.g. Carnec *et al.*, 1996; Wright & Stow, 1999). More recently, spatial distributions of heave in coal measures rocks (e.g. Sowter *et al.*, 2013; Bateson *et al.*, 2015; Sowter *et al.*, 2018; Gee *et al.*, 2019) and temporal correlations between the rise of mine water and deformation time-series (e.g. Cuenca *et al.*, 2013; Gee *et al.*, 2017) have been observed over abandoned coalfields.

The monitoring of groundwater rebound in abandoned coalfields requires a dense, regular spatiotemporal sampling of ground deformation measurements. This is because the response to hydrostatic pressure changes caused by pumping can be highly spatially variable due to differences in the compressibility, thickness and confinement of the aquifer volume (Castellazzi *et al.*, 2018). However, the obtained spatial distribution and density of

DInSAR measurements can be severely affected by phase decorrelation or incoherence (Crosetto *et al.*, 2010). This effect is most prevalent in higher frequency radar bands (e.g. C-band) and incoherence is pervasive over agricultural land, forests, semi-natural areas and wetlands. This is particularly constraining for both persistent scatterer interferometry (PSI) and small baseline techniques. Small baseline methods have proven to achieve meaningful results in areas typically unfavourable for DInSAR analysis (e.g. Lu & Kwoun, 2008), however, the density and distribution of measurements is still limited (Osmanoğlu *et al.*, 2016). Furthermore, data availability has been an additional historical limitation where it is crucial to have sufficient data acquisitions spanning a deformation event at an appropriate revisit time for a reliable analysis.

The potential of DInSAR has continued to improve over time with many advancements in processing algorithms and increasing data availability from SAR orbital systems. In this regard, two notable advances are the development of the Intermittent Small Baseline Subset (ISBAS) (Sowter *et al.*, 2013; Sowter *et al.*, 2016) processing method and the launch of the Sentinel-1 satellite. The ISBAS method is an adapted version of the SBAS method (Berardino *et al.*, 2002) that is capable of computing velocities over unfavourable land cover types to return a spatially distributed set of deformation measurements with near complete ground coverage (Cigna & Sowter, 2017). Sentinel-1 is a two-satellite constellation carrying a C-Band (5.5 cm wavelength — 5.4 GHz) SAR payload which provides conflict-free data every 6 days in Europe and at least 12 days for the majority of the global landmasses (Torres *et al.*, 2012). Characterising and predicting the rise of AMD is a global challenge facing parts of Europe (Gee *et al.*, 2017), Africa (van Tonder *et al.*, 2007), Asia (Liu *et al.*, 2020), Australia (Wright *et al.*, 2010) and the Americas (Gammons *et al.*, 2010), particularly as the demand for coal

declines in favour of more sustainable energy sources. With this in mind, this study aims to propose a cost-effective method to model groundwater rise in recently abandoned coalfields using DInSAR for the purpose of identifying where problems associated with mine water rebound may manifest. The specific objectives are to:

- (i) generate a forward analytical model to predict the change in thickness of the strata and, hence, determine surface movement, based upon measurements of groundwater change from monitoring boreholes;
- (ii) calibrate and validate the model using ISBAS DInSAR;
- (iii) invert the DInSAR measurements to provide an estimate of the change in groundwater levels with detailed and near-complete spatial coverage across the coalfield;
- (iv) utilize the inverted rates to estimate the time it will take for groundwater to discharge out of the Coal Measures rock.

These objectives provide the structural sub-headings used in the following Methods and Results and Discussions sections.

2. Study Site & Materials

2.1. Land Cover

The study site comprises ~2000 km² and covers the counties of Derbyshire and Nottinghamshire, UK (Figure 1). Land cover is largely rural, dominated by agricultural land (50%) with patches of pastures (21%), forests (7%), semi-natural areas (<2%), and wetlands

(<1%) (European Environment Agency, 2012). Artificial surfaces (20%) predominantly correspond to the city of Nottingham in the south and towns of Mansfield and Chesterfield in the centre and north-west, respectively. Water bodies make up less than 1% of the total land cover. Topographically, the study site is located between the Peak District at the southern end of Pennines hill and mountain range in the west, where the elevation reaches a maximum of 380 m above ordnance datum (AOD), and the midlands plains to the east at mean sea level.

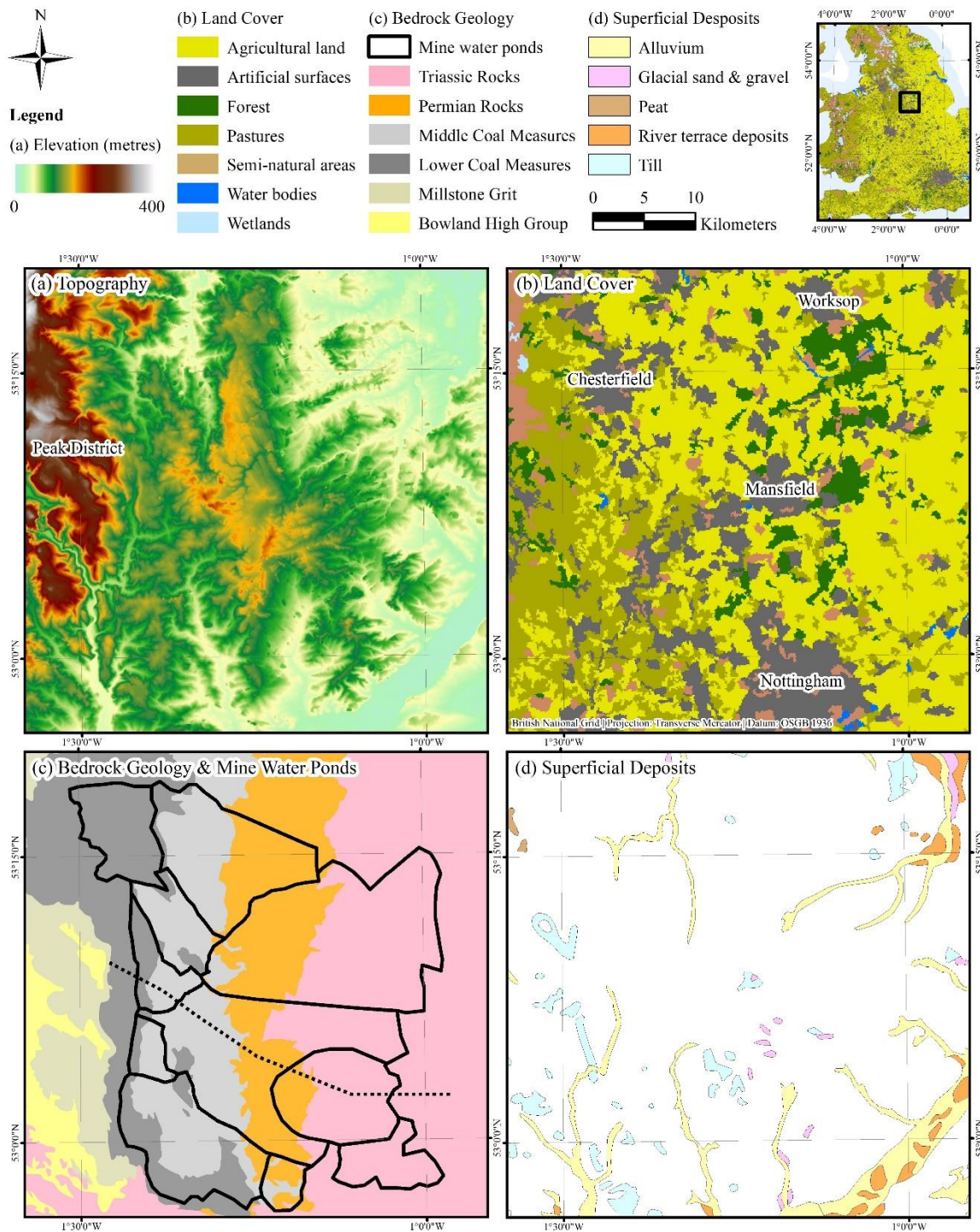


Figure 1. (a) Topography – NEXTMap® DTM at 10 m resolution; (b) CORINE land cover inventory (European Environment Agency, 2012); (c) Bedrock geology at 1:625,000 scale, from BGS Geology 625k (DiGMapGB-625) data; and (d) Superficial deposits at 1:625,000 scale, from BGS Geology 625k (DiGMapGB-625) data. The dashed black line in (c) shows the location of the cross-section in Figure 2. NEXTMap® Britain © 2003, Intermap Technologies Inc. European Environment Agency © 2012. Reproduced with the permission of the British Geological Survey © NERC. All rights Reserved.

2.2. Geology

The study area lies to the east of the Pennine Dinantian-Namurian anticlinal ridge (Figures 1 and 2). The Coal Measures Group (CMG) are dominated by argillaceous strata with alternations of sandstone, grey siltstone and grey mudstone with frequent coal seams and seatearth horizons. Groundwater movement largely occurs via secondary permeability through fractures, given that the carboniferous strata are extensively faulted which act to either increase permeability or prevent hydraulic connectivity (Holliday, 1986). The Nottinghamshire Coalfields have been extensively worked since the early 1800s until the last deep mine, Thoresby, was closed in July 2015. Over thirty separate seams have been mined, and the extraction of large volumes of coal and adjacent rock, associated fracturing and collapse of *in situ* strata, generation of roadways and entry shafts, and areas of goaf generate a complex combination of disturbed and undisturbed strata. The most exploited horizon is the Top Hard seam and neighbouring collieries are frequently linked via the working of this seam from different directions (Dumpleton *et al.*, 2001). The CMG dip regionally east under the East Midlands shelf, which is formed of Permian and Triassic strata and ranges between 50 m to 200 m in thickness from west to east. The bedrock is overlain with superficial deposits that are only up to a few metres thick (Charsley *et al.*, 1990).

The geological parameters required for establishing a groundwater model are the porosity and compression index of the CMG. The porosity was determined as 0.134, calculated as the

mean of 236 measurements of the Pennine CMG from the National Geotechnical Properties Database of the British Geological Survey (BGS). No laboratory samples were available to determine the compression index, therefore a value for dense sand of 0.005 was defined according to the literature (Jain *et al.* 2015). In addition, a digital elevation model (NEXTMap® DTM) and the 3D extent of the top of the Middle Coal Measures formation (Figure 2) was required, with the latter taken from the BGS 1:250,000 3D geological models of the Pennine Basin (Hulbert & Terrington, 2014a; b).

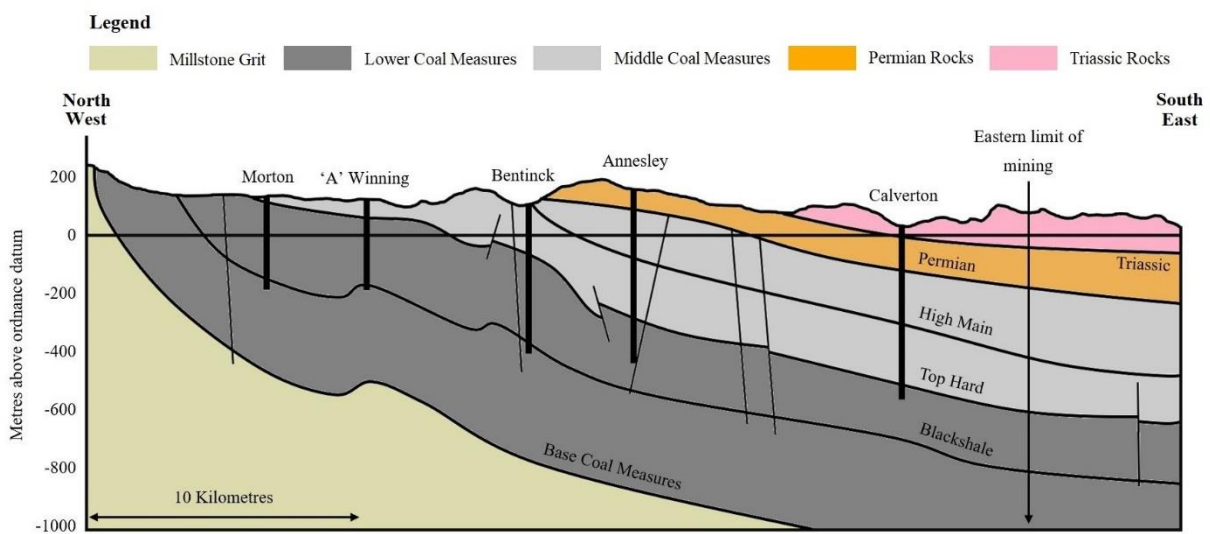


Figure 2. Cross-section of the Nottinghamshire Coalfield. The location is marked on Figure 1c. The thick vertical black lines represent shaft locations and thinner off vertical black lines represent faults. The high main seam demarcates the upper limit of mining. The base of the Top Hard and Blackshale seams for the areas east and west of Annesley-Bentinck, respectively, indicates the base of the zone of enhanced permeability due to mining induced fractures (adapted from Dumpleton *et al.*, 2001).

2.3. Hydrogeology

Mining activities have substantially altered the permeability of the CMG, whereby hydraulic connectivity has been generated between previously isolated horizons and abandoned saturated workings (Banks, 1997). The Nottinghamshire Coalfield is divided by the NW–SE Hardsoft-Mansfield anticline into northern and southern fault-bound sections, which can be further sub-divided into mine water ponds (Figure 3). Younger & Adams (1999) introduced the Groundwater Rebound in Abandoned Mineworkings (GRAM) modelling concept, within which the coalfield is simplified into discrete ponds that represent groups of mine workings that are – with respect to rebound – hydraulically analogous. Connectivity within the ponds can be extensive and, hence, these are expected to subside or uplift uniformly at the surface dependant on the associated groundwater regime. Some of the ponds are known to contain sub-ponds which have not been resolved due to a lack of mine water information. Hydraulic connectivity between ponds occurs at different levels between permeable geological features, mining roadways, existing boreholes and areas where adjoining goaf panels collapse. As the groundwater rises, the ponds fill until a connection to another pond is reached and water decants into the neighbouring pond. Connections between ponds alter at depth and therefore ponds can become isolated or connected at different stages of abandonment. Figure 3 shows the expected schematic of groundwater flow. The workings of the deepest mines in the east were very dry, however, they are connected via an extensive network of workings up-dip which receive considerable ingress from rainfall and surface runoff (Rae, 1978). Little is known about the amount of flow, if any, between the deepest mines, since mine water accumulating in shallower workings was pumped to prevent the build-up of water against hydraulic barriers and therefore reduce the risk of inrushes.

Hydrogeological data was provided by the Coal Authority and was available for 21 and 24 boreholes coinciding with the ENVISAT and Sentinel-1 periods, respectively (Table 1). The number and frequency of groundwater measurements vary and where borehole data was incomplete across the epoch, it was linearly interpolated to fit the time-period provided that it covered more than three quarters of the epoch; otherwise it was discarded. Spatially, groundwater measurements are relatively sparse, with no information on levels in the Chesterfield, North Deep, Swanick or Gedling ponds for either time epochs.

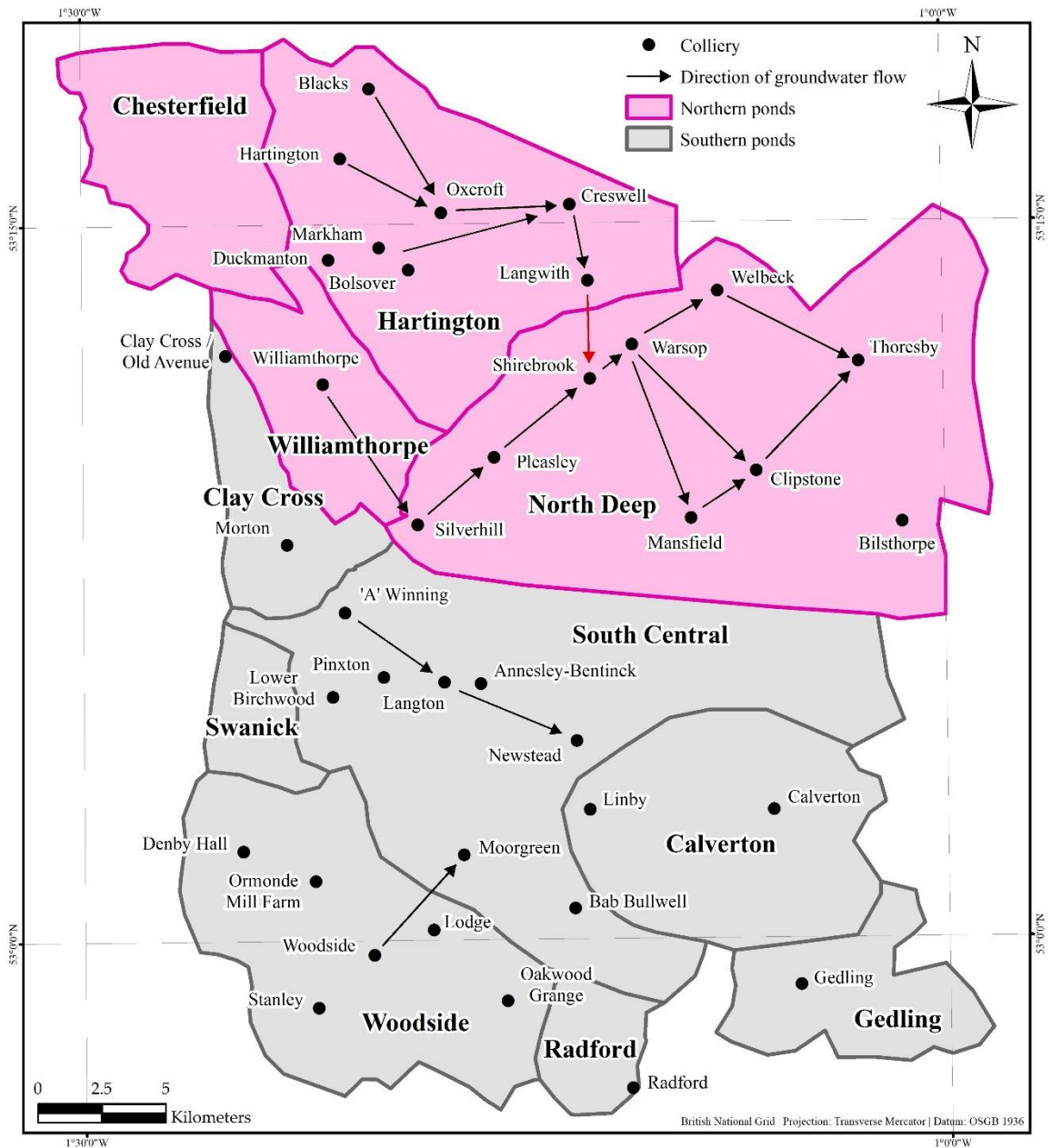


Figure 3. Mine water ponds and expected schematic of flow of groundwater for the Nottinghamshire Coalfield. The red arrow between Langwith and Shirebrook indicates that at present there is very little or no flow between this barrier.

Table 1. Groundwater data for the ENVISAT (November 2002 – November 2009) and Sentinel-1 (May 2015 – April 2019) periods.

Coalfield	Pond	Borehole	ENVISAT (2002 – 2009)								Sentinel-1 (2015 – 2019)							
			No. Measurements	Start Height (Metres AOD)	End Height (Metres AOD)	Head Change (Metres)	Coefficient of Determination (R ²)	Mean Start (Metres AOD)	Mean End (Metres AOD)	Mean Head Change (Metres)	No. Measurements	Start Height (Metres AOD)	End Height (Metres AOD)	Head Change (Metres)	Coefficient of Determination (R ²)	Mean Start (Metres AOD)	Mean End (Metres AOD)	Mean Head Change (Metres)
North	Chesterfield	-	-	-	-	-	-	-	-	-	-	-	-	-	-	-	-	
	Hartington	Blacks	77	2.6	2.8	0.2	0.09	-139.4	-120.3	19.1	12	2.7	15.9	13.2	0.65	-82.3	-29.4	52.9
		Hartington	288	-140.9	-142.6	-1.7	0.16				30	-58.5	14.5	72.9	0.98			
		Duckmanton	39	69.7	69.8	0.1	0.24				-	-	-	-	-			
		Markham	3	-341.4	201.1	140.3	0.98				-	-	-	-	-			
		Oxcroft No.2	161	1.5	-11.8	-13.2	0.82				5	-10.2	15.9	26.1	0.97			
		Creswell	162	-300.3	-301.4	-1.1	0.26				4	-172.5	-95.0	77.6	0.97			
		Langwith	158	-266.9	-257.9	9.0	0.31				23	-172.9	-98.4	74.5	0.99			
Williamthorpe	Williamthorpe	280	-143.7	-147.4	-3.7	0.00	-143.7	-147.4	-3.7	11	-49.0	20.3	69.3	0.91	-49.0	20.3	69.3	
North Deep	-	-	-	-	-	-	-	-	-	-	-	-	-	-	-	-		
South	Clay Cross	Morton	183	33.8	78.3	44.5	0.95	57.9	78.5	20.6	25	88.4	84.8	-3.6	0.16	82.6	82.2	-0.4
		Clay Cross 1	168	56.5	77.4	20.9	0.94				12	79.9	81.7	1.8	0.23			
		Clay Cross 2	161	56.5	76.9	20.4	0.94				12	79.5	79.5	0.0	0.20			
		Old Avenue 3	939	65.2	78.1	12.9	0.74				19	80.3	80.2	-0.1	0.02			
		Old Avenue 4	166	77.4	81.8	4.4	0.55				21	84.9	85.0	0.1	0.18			
		'A' Winning	162	-41.8	44.3	86.1	0.99				162	47.3	36.1	-11.2	0.02			
	South Central	Lower Birchwood	-	-	-	-	-	-175.5	-21.1	154.4	10	55.6	55.1	-0.5	0.15	23.5	35.6	12.1
		Pinxton	-	-	-	-	-				142	27.8	44.7	16.9	0.11			
		Langton	82	-309.2	-86.5	222.7	0.98				155	25.7	44.5	18.8	0.97			
		Newstead	-	-	-	-	-				146	22.5	41.1	18.5	0.96			
		Moorgreen	-	-	-	-	-				141	10.4	34.6	24.2	0.84			
		Babington Bulwell	-	-	-	-	-				132	-25.1	-7.0	18.1	0.83			
	Swanick	-	-	-	-	-	-	-	-	-	-	-	-	-	-	-		
	Woodside	Denby Hall	788	78.2	85.5	7.2	0.22	46.0	50.9	4.9	13	88.8	94.1	6.1	0.33	67.4	66.7	-0.7
		Ormonde (Mill Farm)	565	64.4	68.7	4.3	0.64				9	70.9	76.3	5.4	0.69			
		Woodside	301	16.5	0.3	-16.2	0.00				82	38.5	10.9	-27.6	0.34			
		Stanley	1098	53.5	58.9	5.4	0.27				17	91.7	101.6	9.9	0.20			
Oakwood Grange		1231	17.3	41.0	23.7	0.74	14				47.9	50.6	2.7	0.17				
Radford	Radford	-	-	-	-	-	-	-	-	14	25.1	25.1	0.0	0.00	25.1	25.1	0.0	
Calverton	Calverton	38	-408.9	-377.9	30.0	0.94	-408.9	-377.9	31.0	-	-	-	-	-	-	-	-	
Gedling	-	-	-	-	-	-	-	-	-	-	-	-	-	-	-	-	-	

Table 2. Earth Observation data and ISBAS processing parameters.

Satellite	Geometry	Track	N° of Images	Date Range	Median Revisit (Days)	Max. Orbital Baseline (Metres)	Min. Temp. Baseline (Days)	Max. Temp. Baseline (Days)	Mean Temp. Baseline (Days)	Multilooking (Azimuth: Range)	Coherence Threshold	N° of Interferograms	Interferogram Threshold	Reference Point
ENVISAT	Desc.	366	40	30/Nov/2002 – 28/Nov/2009	35	250	0	1460	618	20 : 4	0.25	240	70	Nottingham City Centre
Sentinel-1	Desc.	154	185	08/May/2015 – 17/Apr/2019	6	45	365		673	6 : 21		3603	370	
	Asc.	132	175	06/May/2015 – 15/Apr/2019		50			674			3558		

2.4. Earth Observation Data

Thirty-nine ENVISAT C-Band Stripmap Level-1 single look complex (SLC) Image Mode products in VV polarisation from descending track 366 were available over the study site (Table 2). There were insufficient acquisitions from the ascending geometry for a reliable analysis. The descending data has a median revisit time of 35 days over a seven-year period (November 2002 – November 2009) regularly distributed throughout the epoch. The incidence angle ranges between 20.1° and 25.9° from near to far range with respect to the surface normal. The products have a pixel spacing of 8 m in slant range and 4 m in azimuth, corresponding to an approximate ground spatial resolution of 25 m in range and 5 m in azimuth. In addition, 185 Sentinel-1 C-Band Terrain Observation with Progressive Scans SAR Interferometric Wide (IW) SLC VV polarized images from descending track 154 and 176 images from ascending track 132 (May 2015 – April 2019) were utilized (Table 2). The median revisit time is much reduced with respect to the ENVISAT data at 6 days. The Sentinel-1 IW products have a pixel spacing 2.3 m in slant range and 13.9 m in azimuth, corresponding to a spatial resolution 5 m in ground range and 20 m in azimuth at scene centre. The incidence angle varies from 29.1° to 46° across the swaths from near to far range.

3. Methods

3.1. Generation of Forward Model using Borehole Measurements

The forward model applies the principle of effective stress (Terzaghi, 1925) and mine water ponds (Younger & Adams, 1999) to calculate the increase in bed thickness (i.e. heave) that

occurs for a given rise in groundwater level. Separate models were set up for the ENVISAT (2002 – 2009) and Sentinel-1 (2015 – 2019) epochs since the two stacks of SAR data were processed separately. The model is treated as a homogeneous matrix, where the initial bed thickness (b_0) (m) was calculated as the depth from the surface to the groundwater level at the start of the modelling epoch (Table 1). The bed thickness was interpolated for each pond based on the borehole measurements. The structure of mines or any of the interseam connections were not considered as their inclusion would introduce an undesired level of complexity to the model that would exceed the scope of the simple approach presented here. As groundwater levels fluctuate over the time-epochs but remain confined to the CMG unit, the model calculates the change in bed thickness of only the CMG unit. It does not consider any compaction of the overlying Permo-Triassic formation. For each pond to determine the rise in groundwater, or change in piezometric head (Δh) (m), across the coalfield over the modelling epoch the borehole measurements were interpolated (Table 1). For ponds where only one measurement was available, a uniform surface was utilized.

The strata is subject to a level of geostatic pressure (p) (kPa), which increases as more material is overlain over time. Geostatic pressure is resisted by the intergranular (effective) stress (p_{s0}) of the rock matrix and the fluid pressure of pore water (p_{w0}) (Poland, 1984):

$$p = p_{s0} + p_{w0} \quad (\text{Eqn. 1})$$

Equilibrium must be maintained in Eqn. 1, thus, an increase in piezometric head increases the pore fluid pressure and decreases the effective stress on the strata. This results in expansion of the strata until equilibrium is again reached. The stress transfer from fluid to rock matrix per unit change in piezometric head was calculated at 10 kPa/m by Poland (1984). The geostatic pressure was calculated from the initial bed thickness (b_0) as:

$$p = 10 \cdot b_0 \quad (\text{Eqn. 2})$$

Poland (1984) estimated for an unconfined aquifer that geostatic pressure is divided as 60% effective stress and 40% pore fluid pressure, whereas for a confined aquifer this is divided as 75% effective stress and 25% pore fluid pressure. In the western exposed coalfield only a single formation exists (the CMG), whilst in the east the CMG is overlain by the Permo-Triassic strata. To account for this, in the western exposed coalfield the CMG is considered unconfined, whereas it is treated as a confined formation where the coalfield is overlain by Permo-Triassic rocks. In the confined formation in the thinnest area of cover the pore fluid pressure is at 25%, which decreased linearly with cover thickness to 10% in the east where cover is thickest.

Following the change in head (Δh), the new pore fluid pressure (p_w) is calculated as:

$$p_w = p_{w0} + 10 \cdot \Delta h \quad (\text{Eqn. 3})$$

and by maintaining the equilibrium in Eqn. 1, the new effective stress (p_s) is:

$$p_s = p - p_w \quad (\text{Eqn. 4})$$

hence, the change in effective stress (Δp_s) can be expressed as a function of the initial geostatic pressure (Eqn. 1) and change in piezometric head:

$$\Delta p_s = p_s - p_{s0}$$

$$\Delta p_s = p - p_w - p_{s0}$$

$$\Delta p_s = p - p_{w0} - 10 \cdot \Delta h - p_{s0} \quad (\text{Eqn. 5})$$

The initial void ratio (e_0) is calculated from the initial porosity (n_0):

$$e_0 = \frac{n_0}{1 - n_0} \quad (\text{Eqn. 6})$$

and after a change in effective stress a new void ratio (e) is calculated:

$$e = e_0 - c_c \cdot \log\left(\frac{p_s}{p_{s0}}\right) \quad (\text{Eqn. 7})$$

as expressed as a function of the initial void ratio (e_0), the compression index (c_c) and the initial (p_{s0}) and new effective stress (p_s). The compression index is a dimensionless parameter that determines the compressibility of the stratigraphic bed and considers the elastic properties of the unit.

The coefficient of volume compressibility (m_v) relates the coefficient of compressibility (a_v) and the initial void ratio (e_0):

$$m_v = \frac{a_v}{1 + e_0} \quad (\text{Eqn. 8})$$

where,

$$a_v = \frac{\Delta e}{\Delta p_s} \quad (\text{Eqn. 9})$$

and Δe is the difference in void ratio.

The change in bed thickness (Δb) is caused by the change in effective stress (Δp_s) and is calculated as a function of the coefficient of volume compressibility (m_v) and the initial thickness of the unit (b_0):

$$\Delta b = s \cdot \Delta p_s \cdot m_v \cdot b_0 \quad (\text{Eqn. 10})$$

where s is a scaling factor to account for predicted inelastic (non-recoverable) deformation.

The response of the strata to changes in piezometric head are dependent on historical pressure changes. Small-scale variations in head (e.g. seasonal effects) are elastic and recoverable so the strata expand and contract in equal measure. When variations in head are greater, the expansion and contraction is bigger which results in inelastic, and non-

recoverable deformation, therefore limiting future expansion and contraction. Coarse grained strata (e.g. sand, gravel) are more likely to maintain equilibrium under increased effective stress due to their rigid skeletal matrix, however, fine-grained material (e.g. clays) are susceptible to high rates of potential compaction due to their plastic nature (Hiscock, 2009). Given the extensive and often variable dewatering regime that has occurred to great depths over many decades in the Nottinghamshire Coalfields and dominance of argillaceous strata within the CMG, it is assumed that the majority of previous compaction is inelastic.

3.2. Calibration & Validation of Forward Model using ISBAS DInSAR Observations

To calibrate the models and calculate the scaling factors, two sets of ground deformation measurements were generated from the ENVISAT and Sentinel-1 data (Table 2). The three stacks, processed separately, were co-registered to a common slant-range coordinate system using an amplitude-based Fast Fourier Transform method (Guizar-Sicairos *et al.*, 2008). In the case of Sentinel-1, each image was deburst and merged prior to co-registration. Short orbital perpendicular baseline differential interferograms were generated following the method proposed by Berardino *et al.* (2002). For ENVISAT, employing a maximum perpendicular baseline of 250 m and maximum temporal baseline of 4 years generated 270 interferograms with a mean temporal baseline of 618 days (Table 2). For the Sentinel-1 analysis, a maximum perpendicular baseline of 45 m and 50 m were applied to the descending and ascending data sets. The baseline was more stringent for the descending dataset to ensure a consistent number of interferograms were generated for both stacks

despite the difference in the number of available images. A minimum temporal baseline of 1 year and no maximum was applied to achieve a similar mean temporal baseline as the ENVISAT stack. A total of 3603 and 3558 interferograms were generated, which have a mean temporal baseline of 673 and 674 days for the descending and ascending stacks, respectively.

An Intermittent Small Baseline Subset (ISBAS) (Sowter *et al.*, 2013; Sowter *et al.*, 2016) analysis was employed due to the dominance of the non-urban land cover. ISBAS is based upon the method of Berardino *et al.* (2002), with a modification in the selection of pixels for analysis. The modification facilitates the retention of pixels which are coherent for only a subset of the total number of interferograms, which is common outside of urban areas. Pixels that fulfil the selection criteria exhibit a defined level of coherence in a minimum number of interferograms. The choice of interferogram threshold determines both the spatial coverage and the precision of the measurement – the standard error. Utilizing an interferogram threshold equal to the total number of interferograms is the equivalent to the method of Berardino *et al.* (2002) and minimizes the standard error of velocity, but at the expense of the density of measurements. The choice of interferogram threshold is a trade-off between coverage and quality, hence, the inversely proportional relationship between the interferogram threshold and the standard error (Cigna & Sowter, 2017). A coherence analysis was employed on the small baseline interferograms, considering all of the image permutations meeting the baseline criteria. No spatial filtering was applied, and coherence was calculated over a multi-looked window of 4 in range and 20 in azimuth for ENVISAT and 21 in range and 6 in azimuth for Sentinel-1. In ground range, the resultant pixels have an approximate pixel spacing of 90 m. A minimum of 70 and 370 interferograms that

exhibited coherence >0.25 were utilized for the ENVISAT and Sentinel-1 analyses, respectively.

Phase ramps attributed to orbital errors were subtracted and phase associated with topography was removed using a 90 m Shuttle Radar Topography Mission (SRTM) DEM (Farr *et al.*, 2007). Coherent and intermittently coherent pixels satisfying the criteria were unwrapped from modulo- 2π phase to relative deformation using a statistical-cost network-flow algorithm (Chen & Zebker, 2001) with respect to a reference point located in Nottingham City centre. The same reference point was used for all data sets and was assumed to be stable due to its urban characteristics and abundant cluster of coherent pixels. After unwrapping, the method is in accordance with that of Berardino *et al.* (2002). The linear velocities are derived from a least squares covariance analysis of the unwrapped phase, which also determines DEM height errors. Standard errors associated with both measurements are calculated from the standard deviation of residuals after fitting. To determine the time-series for each pixel, phase associated with the linear velocities and height errors were removed from the differential interferograms, before being added back after the residual phase components had been unwrapped. The phase velocities between adjacent images were inverted through Singular Value Decomposition. Phase was subsequently integrated to derive the phase at each acquisition interval before temporal high-pass and spatial low-pass filters compute and remove atmospheric components. Modulo- 2π phase time-series are then converted to deformation time-series.

Sufficient ENVISAT data was only available from the descending geometry so, on the assumption that horizontal motion is negligible, the ENVISAT deformation data were projected into the vertical by means of dividing by the cosine of the incidence angle. For

Sentinel-1, the descending time-series were linearly interpolated to the dates of the ascending data before the vertical (d_{vert}) and horizontal (d_{Hor}) components of motion were resolved for both the average velocities and time-series, on the assumption that there is negligible motion in the north-south direction:

$$d_{vert} = \frac{(-\sin\theta_{Desc} \cdot \cos\phi_{Desc} \cdot LOS_{Asc}) + (-\sin\theta_{Asc} \cdot \cos\phi_{Asc} \cdot LOS_{Desc})}{(-\sin\theta_{Asc} \cdot \cos\phi_{Asc} \cdot \cos\theta_{Desc}) - (\cos\theta_{Asc} \cdot \cos\phi_{Desc} \cdot \sin\theta_{Desc})} \quad (\text{Eqn. 11})$$

$$d_{Hor} = \frac{(\cos\theta_{Desc} \cdot LOS_{Asc}) + (-\cos\theta_{Asc} \cdot LOS_{Desc})}{(-\sin\theta_{Asc} \cdot \cos\phi_{Asc} \cdot \cos\theta_{Desc}) - (\cos\theta_{Asc} \cdot \cos\phi_{Desc} \cdot \sin\theta_{Desc})} \quad (\text{Eqn. 12})$$

where θ is the incidence angle from surface normal, ϕ is the azimuth track angle and LOS are the line-of-sight velocity measurements. The superscript indicates whether the parameter corresponds to the ascending (*Asc*) or descending (*Desc*) geometry.

The DInSAR average velocities were utilized to calibrate the forward model. Where there is a notable rise in groundwater, the rise is observed to occur linearly over time. For example, over the ENVISAT and Sentinel-1 epochs the coefficient of determination (R^2) is on average 0.93 and 0.94, respectively, for cases where groundwater rises more than 20 m. Similarly, the time-series data showed that in areas of heave the DInSAR measurements were principally linear which also provides an indication that the observed heave is attributable to groundwater rise. Accordingly, it is appropriate to utilize the average velocities for comparison and calibration (Table 1). In this study, an attempt was not made to utilize the time-series to account for variable pumping rates, however, this could be implemented on a pointwise basis at the borehole locations (e.g. Bateson *et al.*, 2009). To perform calibration, a 1D forward model was generated at each borehole – excluding those located in areas of mining subsidence. The scaling factor(s) that minimised the root mean square error (RMSE) between the modelled measurements and 95th percentile of the DInSAR average velocities

within the surrounding 1 km of the borehole were calculated. The mean scaling factor was taken for each pond. Whilst this approach achieved realistic results in most ponds, some scaling factors were manually adjusted to account for the fact that heave caused by a change in groundwater does not always directly manifest at the borehole location. Instead, it can arise elsewhere within the mine complex and failure to account for this could lead to erroneous calibration. It was clear that when the scaling factor was too low, the average velocities generated by the forward model were too small and, consequently, the inverse map of groundwater rise was unrealistically high. Conversely, when the scaling factor was too high, the velocities in the forward model were similarly too high and the inverse map improbably small. Finally, to provide a quantitative comparison between the forward model and DInSAR average velocities the residuals were calculated by subtracting the modelled deformation from the DInSAR measurements.

3.3. Inversion of ISBAS DInSAR Observations to Estimate Groundwater Rise

To provide a quantitative estimate of groundwater rise (Δh) across the entire coalfield, an inversion of both the average DInSAR velocities and the displacement time-series was implemented as:

$$\Delta h = \frac{1}{10.s} (p - p_{so} - p_{wo} - \left(\frac{\Delta b}{m_v.b_0}\right)) \quad (\text{Eqn. 13})$$

where the DInSAR measurements are utilized to determine the change in bed thickness (Δb).

The change in bed thickness was calculated by multiplying the average velocities by the length of the DInSAR time epoch to determine the cumulative deformation, whereas for the time-series each relative height change was inverted. In addition, the cumulative standard

errors of the average velocities were inverted to provide an estimate of how the measurement error of the DInSAR translates into error in the estimate of groundwater rise.

3.4. Estimate of Time Until Discharge using Inverted Map of Groundwater Rise

The inverted average rate of rise of the Sentinel-1 data was utilized to calculate the time it would take for groundwater to reach the top of the CMG and either discharge at the surface, where the CMG are unconfined, or infiltrate the Permo-Triassic formation. Groundwater recovery curves in most hydrogeological environments, including studies of mine water rebound, follow a shape that conforms to an exponential function. The recovery of mine water is a non-linear process because as the head difference between the formerly dewatered and now recovering strata and surrounding aquifers reduces, the head-dependant inflow also reduces. Hence, the rate of rebound decreases exponentially with time (Younger & Adams, 1999).

It is possible to predict mine water rebound by fitting an exponential curve to early rebound data, however, this is particularly challenging as it assumes that the reduction in head-dependant inflow into the voids of the recovering strata occur at the same rate for entire rebound period. This assumption rarely holds – for instance, the curve might be fit to data for a period when an extensively worked lower seam of relatively high specific yield was flooding. In this case, once the mine water reaches the roof and proceeds into the strata of lower permeability, rebound would accelerate and thus deviate from the assumed exponential function. Rebound might take on an exponential function again once it reaches a higher seam, however, rebound will ultimately occur sooner than predicted. Alternatively, if

the curve is fit to data related to the rapid filling of a seam interval, then rebound will occur later than predicted (Younger & Adams, 1999). Accounting for such processes requires detailed geological, mining and hydrogeological data which are often unavailable.

In Britain, linear projections are utilized by the Coal Authority for the management of mine water, as this provides a scenario towards the worst-case; one in which rebound occurs more rapidly than in reality, which affords more time to implement pumping and treatment schemes. Such an estimate is preferable over an exponential projection that might erroneously indicate an area is not at risk. In line with this, the estimate of time until discharge was calculated by dividing the depth of the groundwater from the top of the CMG at the end of the Sentinel-1 period by the inverted yearly rate of groundwater rise. The depth of groundwater at the end of the Sentinel-1 period was interpolated from the boreholes for each pond.

4. Results & Discussion

4.1. Generation of Forward Model using Borehole Measurements

The results from the initial models showed good spatial agreement with areas of heave identified in the DInSAR data, however, large differences occurred in the magnitude of deformation. Such differences occur due to the choice of parameters; for example, whilst the value of porosity has been taken from real samples, the extraction of vast areas of strata and resultant void space will act to likely increase this value. The compression index was taken from literature and even had actual measurements been utilized, the CMG are a highly variable complex multilayer aquifer so samples may not be representative of the entire formation. Additionally, the response of the strata to pressure changes is also dependant on

historical elastic and inelastic deformation, the degree of which is unknown, hence, leading to uncertainties.

4.2. Calibration & Validation of Forward Model using ISBAS DInSAR Observations

The average annual velocities identified over the ENVISAT and Sentinel-1 periods are shown in Figure 4. The near complete spatial coverage (~94%) of the ISBAS measurements facilitates a comprehensive characterisation of the deformation occurring over the coalfield. Areas of spatially correlated heave are measured in both data sets and occur because of rising groundwater. The temporal evolution of deformation between the ENVISAT and Sentinel-1 data concur with the timeframes of coalfield abandonment. For example, rebound in the northern coalfield has only recently commenced. Over the ENVISAT period the area is relatively stable, and pumping was performed in the west of the Hartington and Williamthorpe ponds to prevent infiltrated groundwater migrating downdip. Following the closure of Welbeck in May 2010, pumping has gradually been reduced allowing the deeper easterly mine workings to flood. At present there is very little flow across the barrier between the Langwith and Shirebrook, located in the North Deep pond. As a result, mine water is rising at Creswell and Langwith and heave is identified in the Sentinel-1 DInSAR. The barrier between Williamthorpe and Silverhill is known to leak and is allowing some flow into the North Deep pond, as evidenced from modelling by the Coal Authority in 2016/17. When Thoresby was closed in 2015, aside from the expected flow and flooding from the make of water from the mine workings, there was no evidence for notable large or increased flows coming from Williamthorpe, suggesting that pumping at Williamthorpe had prevented significant down-dip decant. Rebound is soon expected in the North Deep pond,

however, no heave is observed over the period 2015 – 2019. This suggests that the connections with the westerly ponds are not present as anticipated, or that the groundwater levels have not yet reached the depth of the connections. Future DInSAR monitoring of this area will help to identify such a change, where groundwater has not yet reached the bottom of the monitoring borehole in the North Deep pond. In the southern coalfield, the most easterly up-dip measures around Morton and 'A' Winning recovered during the 2000s where heave is identified, and are subsequently stable once recovered and pumped in the 2010s.

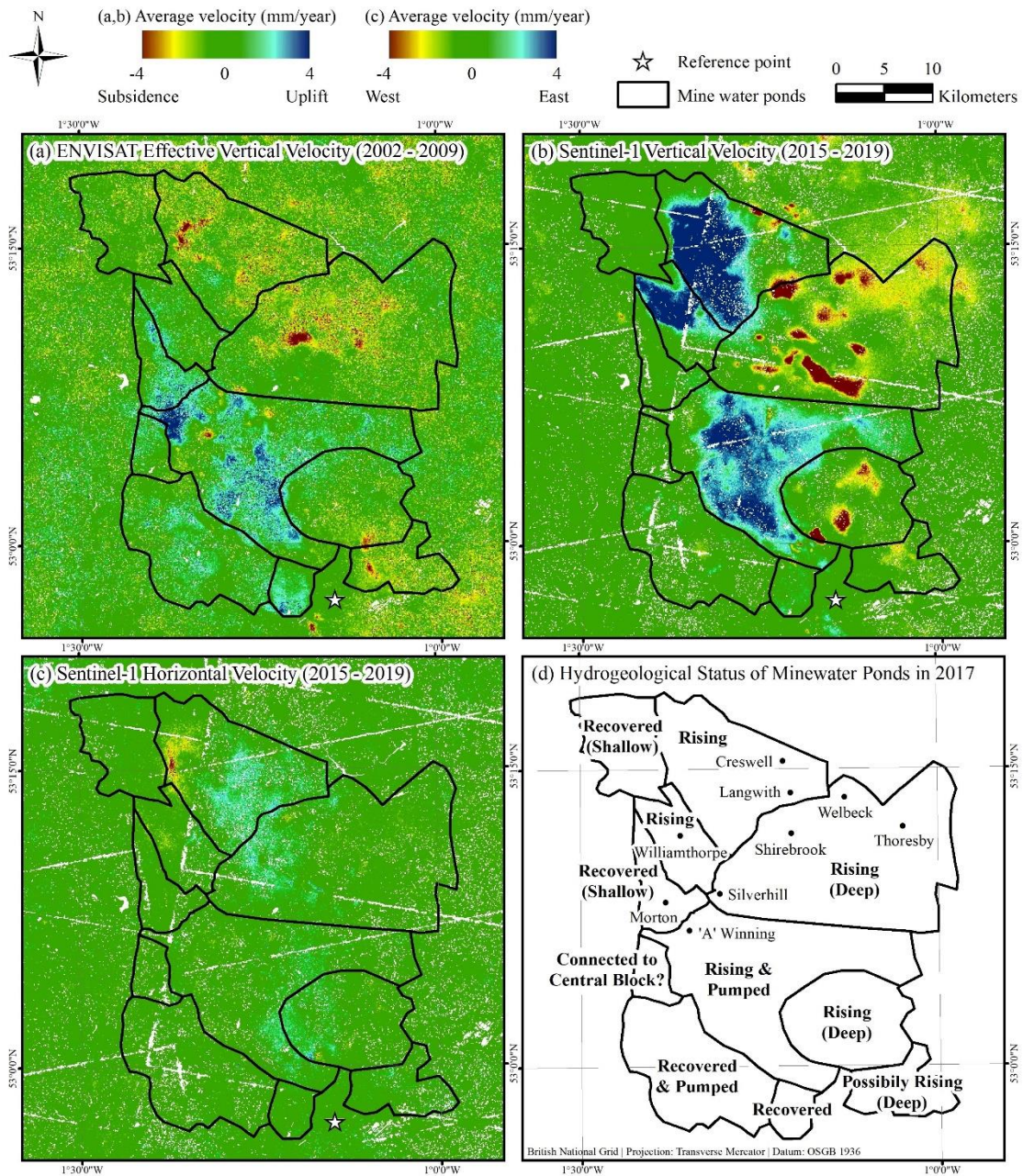


Figure 4. (a) ENVISAT effective vertical velocities (mm/year); (b) Sentinel-1 vertical velocity (mm/year); (c) Sentinel-1 horizontal velocity (mm/year); and (d) Hydrogeological status of minewater ponds in 2017.

At the regional scale of the entire coalfield, the calibrated forward models of heave show good agreement with the DInSAR surface deformation measurements (i.e. heave is observed in ponds where groundwater is rising) (Figure 5). Over the ENVISAT epoch (2002 – 2009),

the modelled heave primarily occurs in the southern coalfield, within the South Central pond, driven by rebound at 'A' Winning and Langton. The DInSAR similarly identifies heave in South Central, although the rates are spatially variable in this relatively large pond suggesting South Central could contain sub-ponds. This evidences the simplification that the concept of ponds are relative to the actual geological setting. In the north the modelled heave is small. The DInSAR indicate that this pond is relatively stable, although there is a region of subsidence over the Markham borehole with an area of heave further to the south.

Over the Sentinel-1 epoch (2015 – 2019), heave occurs in the north coalfield within the Hartington and Williamthorpe ponds, in areas experiencing some of the largest recovery of groundwater (Figure 5). Hydraulic connectivity within the Hartington and Williamthorpe ponds are extensive. The DInSAR measurements concur with the modelled deformation, showing that heave is geologically bound by the outcropping of Pennine Middle Coal Measures. Most significantly, within the Hartington pond both the DInSAR and modelled deformation show that surface heave is of a lower velocity where the coal measures dip under the Permo-Triassic horizon. Where the CMG is confined, the DInSAR identifies lesser movement, mostly in close proximity to the boreholes at Creswell and Langwith where groundwater is rising. Crucial to this verification was the near-complete coverage (~94%) of the ISBAS DInSAR measurements in an area dominated by agricultural land where coherence is intermittent. If a conventional SBAS analysis had been utilized, the ground measurement coverage would not have been sufficient to validate the change in rate of heave of the forward model where the CMG become confined (Figure 6). Furthermore, calibration of the model would have been more challenging because 70% of the boreholes are situated within intermittently coherent pixels.

Heave also occurs in the DInSAR and the model in the South Central pond, in which groundwater levels are rising. To the west of the pond heave is not measured in the DInSAR in proximity of 'A' Winning where pumping occurs up-dip to control the levels at Langton and Newstead. In South Central heave is bound to the north by Hardsoft-Mansfield anticline which divides the northern and southern coalfields, to the south by a narrow but complex anticlinal zone which divides the South Central pond from the Woodside and Radford ponds (Dumpleton *et al.*, 2001), and to the east by the Calverton pond, despite significant mine water pressure on the barriers (>200 m). As expected, the recovered ponds of Clay Cross, Radford and Woodside are characterised as stable by the DInSAR and the model. Some heave is identified by the DInSAR in close proximity to the boreholes at Denby Hall, Ormonde Mill Farm and Lodge Erewash within the Woodside pond, which is indicative that whilst Woodside has recovered, it is still pumped to prevent mine water discharging at the surface and/or flowing into South Central.

Unfortunately, no ground truth with sufficient spatial and temporal sampling at the required accuracy and precision is available to verify the DInSAR results. However, one of the great advantages of DInSAR is the ability to provide historical and current ground deformation measurements in areas where there is limited or no ground truth data. Prior ISBAS measurements have been validated in urban and rural environments, providing confidence in the method (e.g. Gee *et al.*, 2016; Alshammari *et al.*, 2019; Gee *et al.*, 2019; Grebby *et al.*, 2019). Over the Nottinghamshire Coalfields, the temporal evolution of deformation between the ENVISAT and Sentinel-1 data and the quantitative comparison between the deformation measured by the forward models and DInSAR confirm that the heave is caused by the recovery of mine water. No groundwater data is available to generate

the forward model in several ponds, however, given the agreement between the DInSAR and model, the DInSAR can be utilized to infer the status of rebound. For instance, during the ENVISAT epoch heave is measured in Radford although no borehole measurements are available for this period (Figure 5). The pond is known to have rebounded by the Sentinel-1 epoch (Table 1; Figure 4d) so the DInSAR indicate that recovery occurred partly or wholly between 2002–2009.

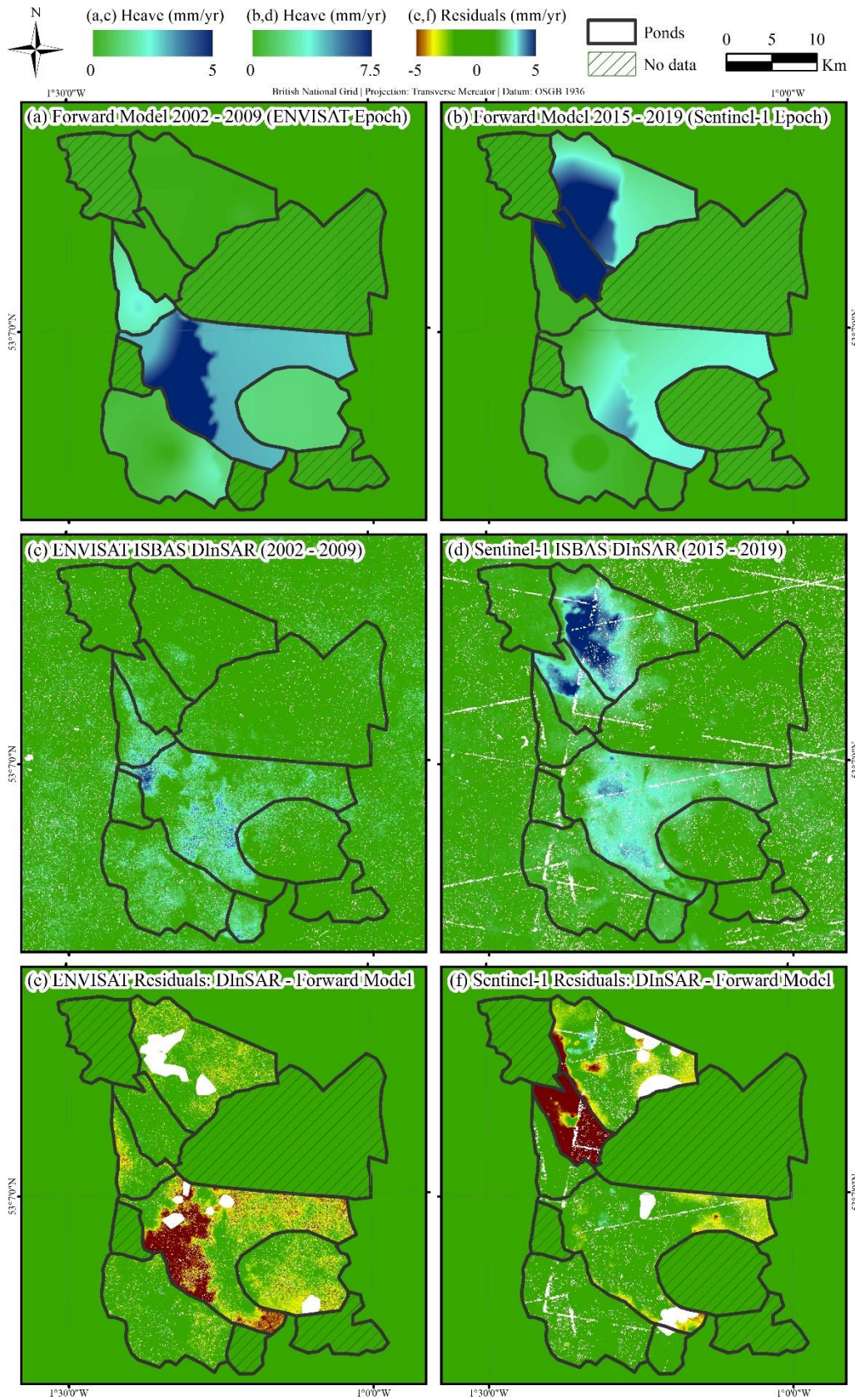


Figure 5. Calibrated forward models for the: (a) ENVISAT and (b) Sentinel-1 time epochs. Intermittent SBAS DInSAR analysis for the: (c) ENVISAT and (d) Sentinel-1 time epochs. Residuals between ISBAS DInSAR and

forward models for the: (e) ENVISAT and (f) Sentinel-1 time epochs. Red and blue indicate respective underestimation and overestimation of heave by the DInSAR relative to the model. Areas of notable subsidence identified by the DInSAR have been masked from the residuals.

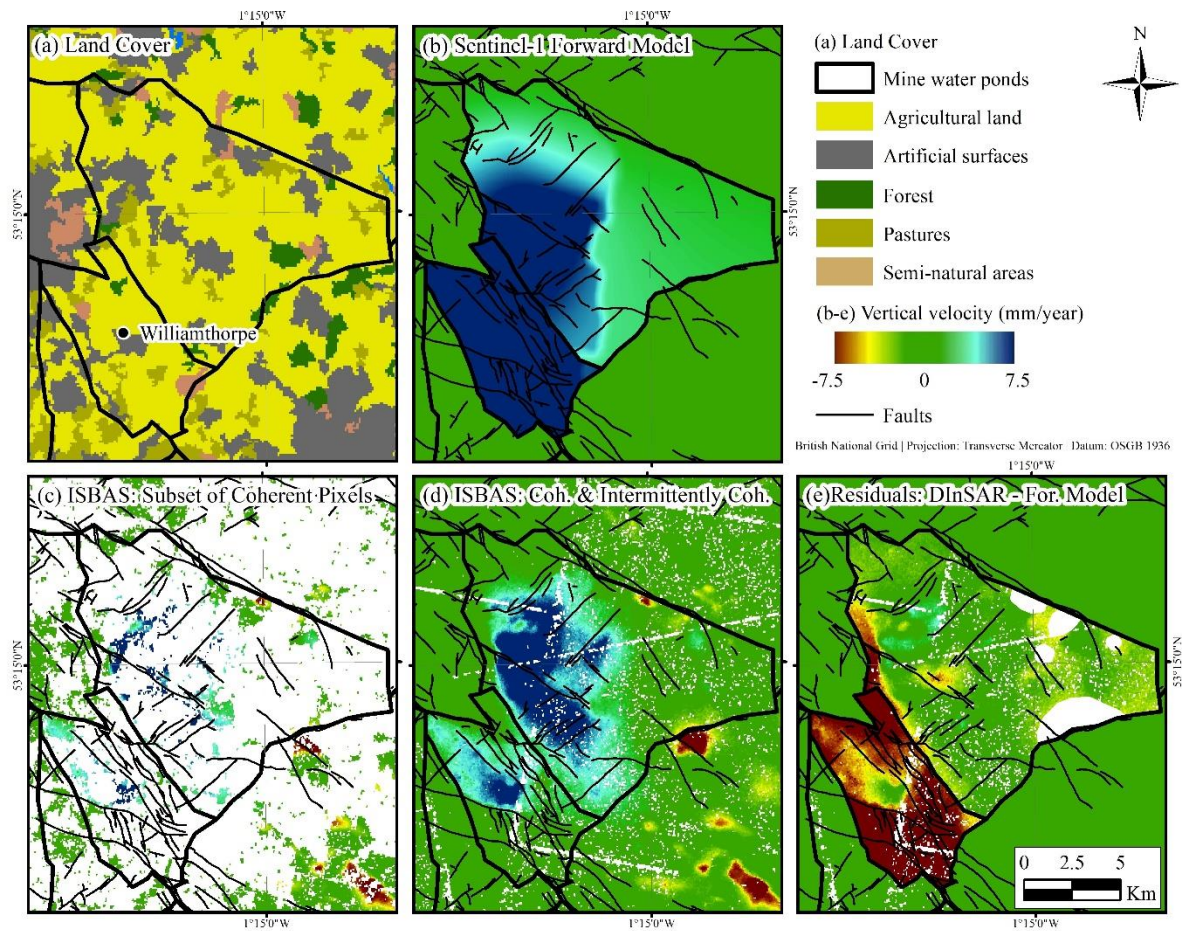


Figure 6. Fault-bound motion and variable deformation within the Hartington and Williamthorpe ponds, measured over the Sentinel-1 period: (a) CORINE land cover inventory (European Environment Agency, 2012); (b) Forward model (mm/year); (c) Sentinel-1 average vertical velocities (mm/year) for the subset of coherent pixels only; (d) Sentinel-1 average velocities (mm/year) for all pixels (coherent and intermittently coherent). Residuals between ISBAS DInSAR and forward models. Red indicates underestimation of heave by the DInSAR relative to the model and blue indicates overestimation by the DInSAR relative to the model. Areas of notable subsidence identified by the DInSAR have been masked from the residuals. European Environment Agency © 2012.

4.3. Inversion of ISBAS DInSAR Observations to Estimate Groundwater Rise

The adoption of ponds to characterise rebound in the coalfield is a practical, albeit necessary, simplification of the actual hydrogeological setting for the forward modelling. Whilst at the regional coalfield scale the forward models show a good level of agreement with the DInSAR measurements, the variability in groundwater rise has to be interpolated, or a single value input for an entire pond where only a single borehole exists. The complex and extensive network of mine workings and poor spatial sampling of the boreholes means that groundwater rise between boreholes is not likely to be realistically characterised. For example, over the Sentinel-1 period within the Williamthorpe pond there is variability in the groundwater levels where heave is confined due to the presence of impermeable faults (Figure 6d,e). The residuals between the forward model and DInSAR observations tend towards zero in the area surrounding the borehole, however, because of the variability in groundwater levels large residuals, up to -10 mm/year, occur in the south of the pond. Similarly, due to the variability of rebound within South Central over the ENVISAT epoch residuals of up to -8mm/year are measured (Figure 5). The near-complete spatial sampling of the ISBAS DInSAR surface measurements can capture the groundwater variability, hence, once inverted the change in groundwater levels are characterised in greater detail than the boreholes can solely achieve across the coalfield.

The inverted DInSAR measurements assume that heave occurs solely as a result of rising groundwater, which may not always be the only cause of the observed ground motions.

However, it is a reasonable assumption given that the spatially correlated heave is delimited by the structural geology and has been validated by the forward models (Section 4.2). The model can be theoretically utilized to predict a drop in groundwater levels. Notably, there are areas where subsidence occurs due to groundwater depletion at boreholes where groundwater has been pumped, for example, in close proximity to Woodside and 'A' Winning over the Sentinel-1 period (~ -2 mm/year). However, groundwater depletion does not cause many of the detrimental problems associated with rebound (e.g. surface water pollution, localised flooding, pollution of overlying aquifers), hence, the purpose of the study is to identify where the problems associated with rebound may manifest. There are also localised hotspots of subsidence that are either known to be or likely to be related to mining induced collapses (e.g. the North Deep and Calverton ponds). Where such subsidence processes are transpiring an estimate of groundwater rise cannot be generated and so these areas are not considered and were masked from the inverse model.

The average inverted rates are shown in Figure 7 and the average of all the inverted time-series in the surrounding 1 km of the boreholes of Hartington, Williamthorpe and Morton are shown in Figure 8. The inverted measurements provide a more realistic estimate of the rise in groundwater than previous simple correlations that universally determine a value of groundwater rise per unit of surface deformation (e.g. Banton *et al.*, 2013). A change in bed thickness within the CMG would plausibly have less of an effect at the surface when the CMG is overlain by successive strata and, similarly, a rise in groundwater closer to the surface would be expected to have a greater control on surface deformation than a rise that occurs at depth. The value of groundwater rise per unit of surface deformation is different for every pixel since the inverted estimate considers both the geology and the depth at

which mine water is rising. For example, over the Sentinel-1 period heave measures up to ~10 mm/year around the Williamthorpe borehole which is in a shallow unconfined area, whereas at Creswell, in a deeper confined area, heave is ~3 mm/year (Figure 9a). If only the surface deformation data was considered, it might be erroneously interpreted that groundwater levels are rising ~3-times as fast at Williamthorpe than Creswell. The inverted measurements consider the geology and depth of groundwater and, hence, correctly determines that over the course of the Sentinel-1 epoch groundwater levels rose faster at Creswell (77.6 m) than Williamthorpe (69.3 m) (Figure 9b).

The standard errors associated with the inverted rates are shown in Figure 7b,d. The inverted standard errors are largest when a relatively small rate of heave translates into a large rise in groundwater (i.e. in deep confined areas such as the east of South Central pond over the ENVISAT period and east of the Hartington pond over the Sentinel-1 period). The standard error of the ISBAS velocities are controlled by the number of coherent interferograms, which is in turn predominantly controlled by the land cover. Coherence is less likely to be maintained outside of urban areas, hence, there are less coherent interferograms and the standard errors of velocities are higher. The standard errors of the Sentinel-1 velocities are on average less than the ENVISAT velocities, as a result of the greater number of images available and smaller perpendicular orbital baselines between images. Hence, the inverted standard errors of groundwater rise are controlled by the quantity and quality of SAR data, land cover, the confinement of the CMG, and depth and rate of change of the groundwater.

Again, the near complete ground coverage of the DInSAR measurements afforded by the ISBAS method has been crucial to the inverse mapping. In previous studies where DInSAR

has been utilized to map groundwater level variations, decorrelation over non-urban land cover meant that measurements had to be interpolated to achieve complete coverage before inversion (e.g. Bejar-Pizarro *et al.*, 2017). Whilst the density of measurements is important for modelling, for spatially correlated deformation, achieving a balanced spatial sampling can be more important to successfully characterise the signal of interest (Hanssen *et al.*, 2008). Spatial interpolation is not required to achieve both a high density and regular spatial sampling with the ISBAS method, ultimately leading to a more accurate characterisation of the changes in groundwater levels.

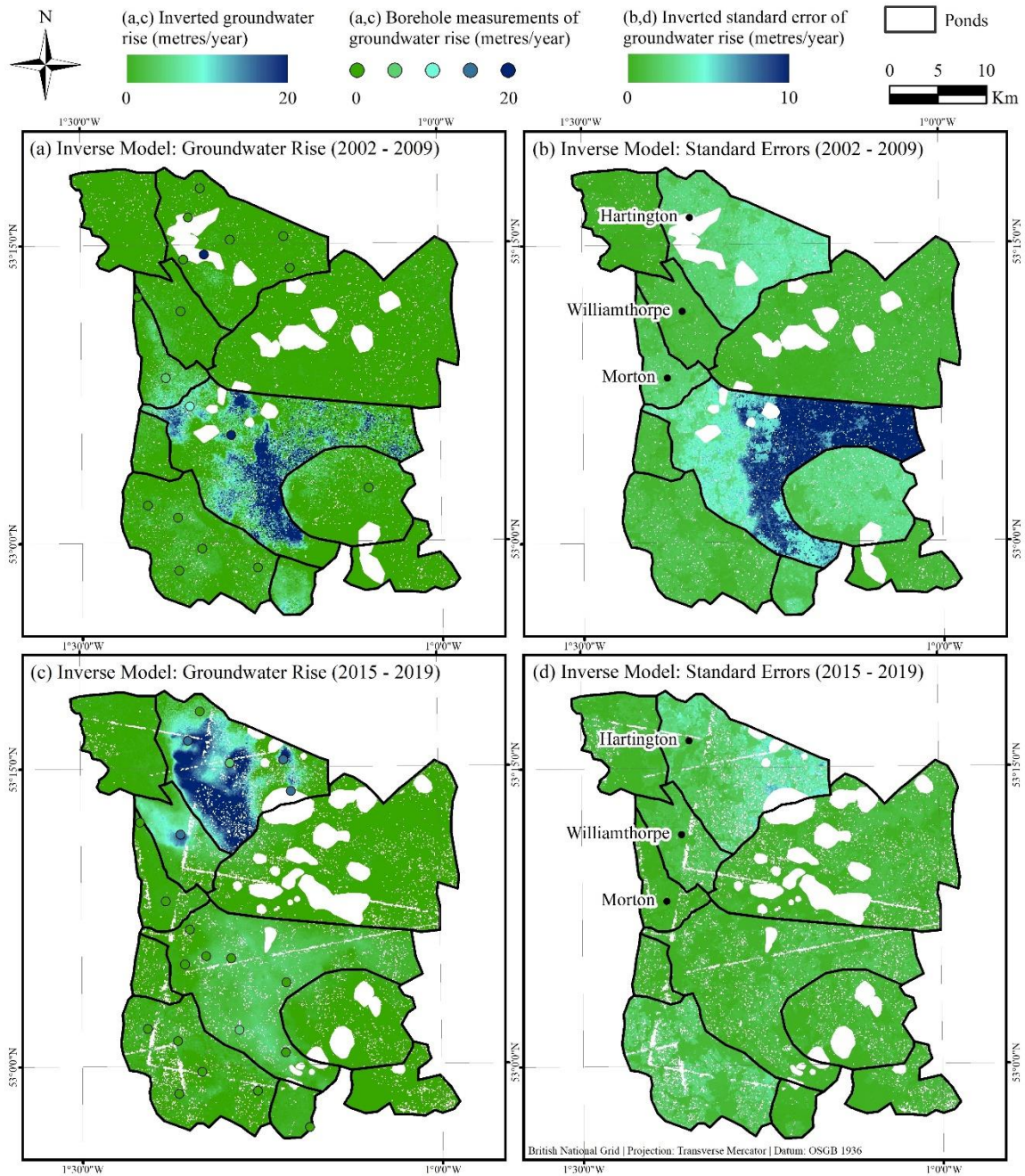


Figure 7. Average change in groundwater levels per year as derived via the inverse model from: (a) ENVISAT ISBAS DInSAR; (b) ENVISAT standard errors; (c) Sentinel-1 ISBAS DInSAR and (d) Sentinel-1 standard errors.

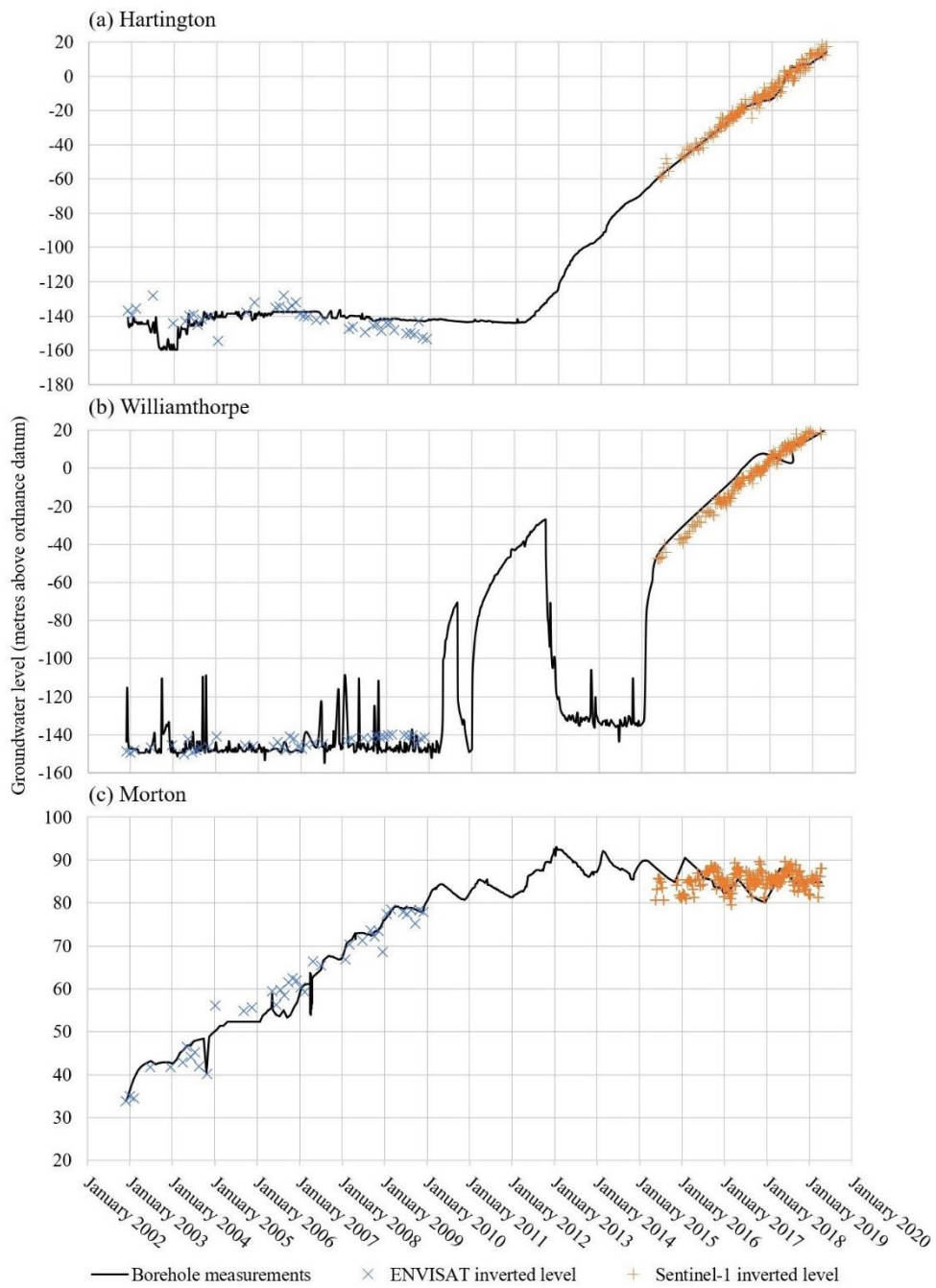


Figure 8. Measured groundwater rise from monitoring boreholes and calibrated inverted groundwater rise from ENVISAT and Sentinel-1 data: (a) Hartington; (b) Williamthorpe; and (c) Morton. The locations of the boreholes are shown in Figure 7.

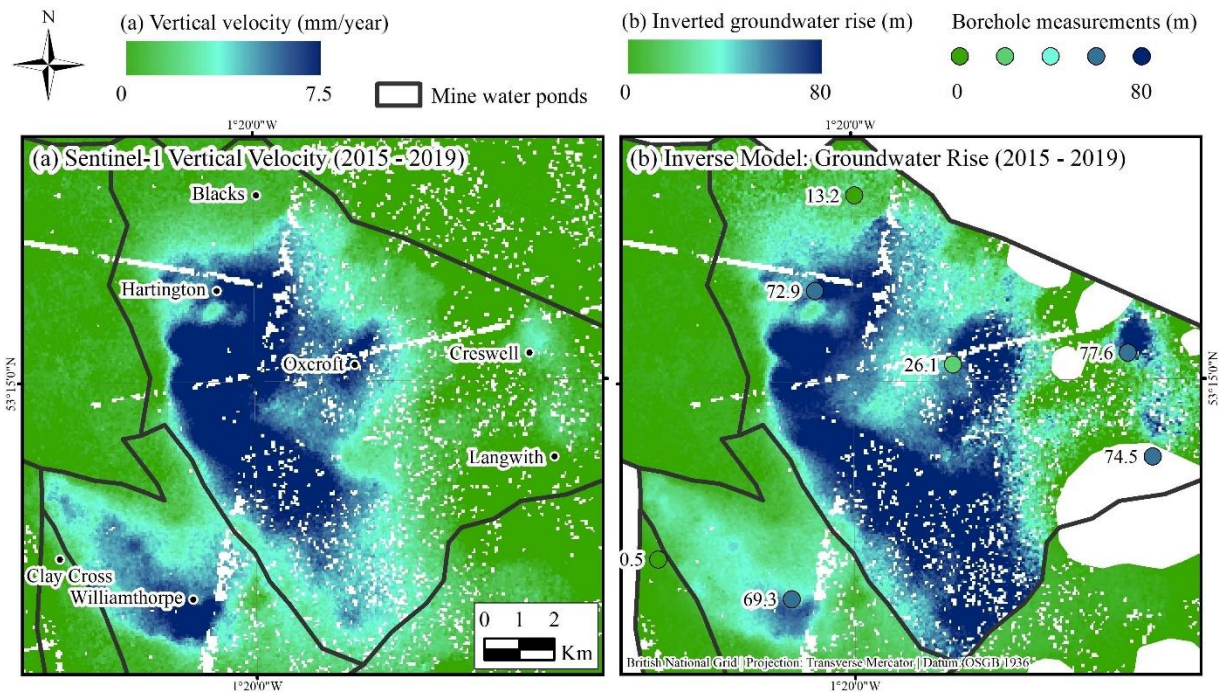


Figure 9. (a) Sentinel-1 vertical velocity (mm/year); and (b) cumulative inverted groundwater rise (m) and borehole measurements over the Sentinel-1 period. Areas of notable subsidence identified by the DInSAR have been masked from the inverse map.

4.4. Estimate of Time Until Discharge using Inverted Map of Groundwater Rise

Figure 10 displays the estimated time until discharge out of the CMG for the worst-case scenario. This assumes that the groundwater regime of the previous four years continues (i.e. the Sentinel-1 period), which might not be the case if a connection to a neighbouring mine is reached or if the Coal Authority decide to pump or stop pumping at selected boreholes. Nevertheless, it will be indicative of where mine water discharges will occur under the current management and can be used to help prevent pollution at the surface or of the overlying Triassic Sherwood Sandstone aquifer, which is a major source of public water

supply for the region. Such an approach could only be implemented effectively for areas where the depth of the groundwater is known at the end of the Sentinel-1 period (April 2019) and requires a regular sampling of borehole measurements, particularly in areas where the CMG dip relatively steeply. This is not the case in the eastern portion of the South Central pond which was, therefore, excluded. The results show that the west of the Hartington and centre of the South Central ponds are predicted to discharge first, in as little six months under the current groundwater regime. In the Williamthorpe pond, discharge is predicted in approximately 18 months at the centre of the pond. Conversely, the effects of pumping are clear in the areas surrounding the 'A' Winning borehole and the entire Woodside pond which are not at risk of discharge.

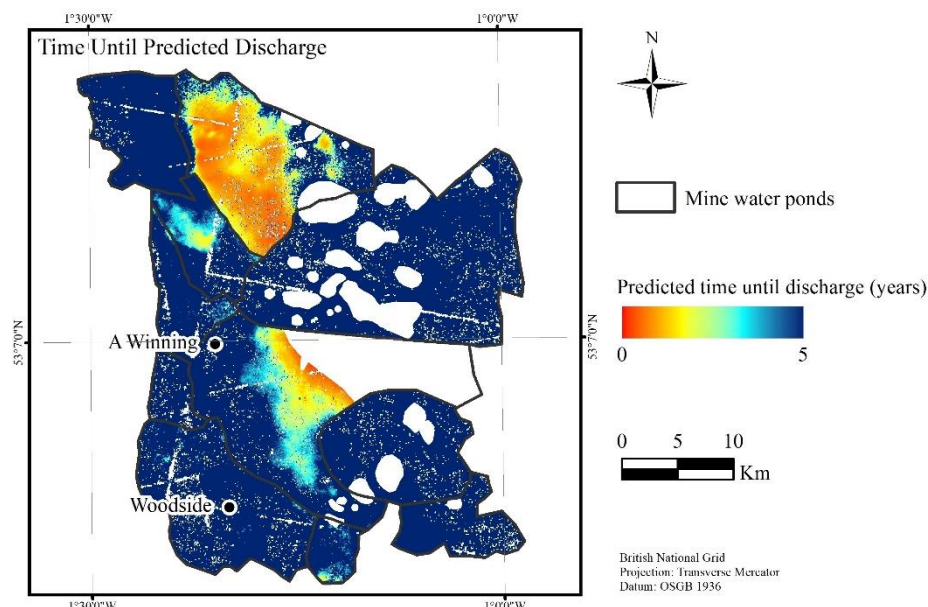


Figure 10. Predicted time until discharge out of the Coal Measures Group, either at the surface or into the Permian-Triassic strata.

5. Conclusion

Characterisation and prediction of hydraulic flow in recently abandoned coalfields is particularly challenging due to inaccurate or incomplete mine plans and sparse monitoring boreholes. In this study, a method based upon the principle of effective stress and concept of mine water ponds was implemented to map variations in groundwater levels using DInSAR. The near complete coverage of the ISBAS deformation measurements was critical to calibrate the model, verify the outputs and provide a spatial quantitative estimate of the rate of groundwater rebound and an estimate of the time it will take for groundwater to discharge out of the Coal Measures rock. Given that many shafts are backfilled following coalfield closure and drilling new deep monitoring boreholes is expensive, the method proposed can provide a valuable cost-effective input into the abandonment strategy to help identify where pumping might be required. It is relatively straightforward to apply and requires few parameters to be estimated, and so, with the aid of the Sentinel-1 archive, has the potential to be readily applied over other recently abandoned coalfields.

Acknowledgements

The research was funded by the GeoEnergy Research Centre (GERC) and Terra Motion Limited. ENVISAT and Sentinel-1 SAR data were provided by the European Space Agency, geological data by the British Geological Survey and hydrogeological data by the Coal Authority. The authors would like to thank Christopher Satterley for his role in the co-

ordination of this research and Andrew Barkwith for useful comments at the beginning of the study. The authors would also like to thank four anonymous reviewers and the Remote Sensing of Environment editorial team who helped to improve the quality of the manuscript. L. Bateson and A. Novellino published with the permission of the Executive Director of BGS.

Conflicts of Interest

The authors declare no conflicts of interest.

References

Alshammari, L., Boyd, D.S., Sowter, A., Marshall, C., Andersen, R., Gilbert, P., Marsh, S. and Large, D.J., 2019. Use of Surface Motion Characteristics Determined by InSAR to Assess Peatland Condition. *Journal of Geophysical Research: Biogeosciences*. 125(1). pp.1-15.

<https://doi.org/10.1029/2018JG004953>

Banks, D., 1997. Hydrogeochemistry of millstone grit and coal measures groundwaters, south Yorkshire and north Derbyshire, UK. *Quarterly Journal of Engineering Geology and Hydrogeology*, 30(3), pp.237-256. <https://doi.org/10.1144/GSL.QJEG.1997.030.P3.06>

Banton, C., Bateson, L., McCormack, H., Holley, R., Watson, I.A., Burren, R., Lawrence, D. and Cigna, F., 2013. Monitoring post-closure large scale surface deformation in mining areas. In *Proceedings of the Eighth International Seminar on Mine Closure*. pp. 97-108. Australian Centre for Geomechanics.

Bateson, L., Cigna, F., Boon, D. and Sowter, A., 2015. The application of the Intermittent SBAS (ISBAS) InSAR method to the South Wales Coalfield, UK. *International Journal of Applied Earth Observation and Geoinformation*, 34, pp.249-257.

<https://doi.org/10.1016/j.jag.2014.08.018>

Bateson, L.B., Barkwith, A.K.A.P., Hughes, A.G., and Aldiss, D. 2009. TerraFirma: London H-3 Modelled Product. Comparison of PS data with the results of a groundwater abstraction related subsidence Model. *British Geological Survey Commissioned Report*, OR/09/032. 47pp.

Béjar-Pizarro, M., Ezquerro, P., Herrera, G., Tomás, R., Guardiola-Albert, C., Hernández, J.M.R., Merodo, J.A.F., Marchamalo, M. and Martínez, R., 2017. Mapping groundwater level and aquifer storage variations from InSAR measurements in the Madrid aquifer, Central Spain. *Journal of Hydrology*, 547, pp.678-689. <https://doi.org/10.1016/j.jhydrol.2017.02.011>

Bekendam, R.F. and Pöttgens, J.J., 1995. Ground movements over the coal mines of southern Limburg, The Netherlands, and their relation to rising mine waters. *Land Subsidence (Proc. Fifth Int. Symp. On Land Subsidence, The Hague, October 1995)*. IAHS Publ. no. 234., pp.3-12.

Bell, J.W., Amelung, F., Ferretti, A., Bianchi, M. and Novali, F., 2008. Permanent scatterer InSAR reveals seasonal and long-term aquifer-system response to groundwater pumping and artificial recharge. *Water Resources Research*, 44(2). <https://doi.org/10.1029/2007WR006152>

Berardino, P., Fornaro, G., Lanari, R. and Sansosti, E., 2002. A new algorithm for surface deformation monitoring based on small baseline differential SAR interferograms. *IEEE Transactions on Geoscience and Remote Sensing*, 40(11), pp.2375-2383.

<https://doi.org/10.1109/TGRS.2002.803792>

Bishop, T.J. and Rushton, K.R., 1993. *Water resource study of the Nottinghamshire Sherwood Sandstone aquifer system of Eastern England*. Mathematical Model of the Sherwood Sandstone aquifer. Report for the National Rivers Authority of England and Wales – Severn Trent Region, Department of Civil Engineering, University of Birmingham.

Carnec, C., Massonnet, D. and King, C., 1996. Two examples of the use of SAR interferometry on displacement fields of small spatial extent. *Geophysical research letters*, 23(24), pp.3579-3582. <https://doi.org/10.1029/96GL03042>

Castellazzi, P., Longuevergne, L., Martel, R., Rivera, A., Brouard, C. and Chaussard, E., 2018. Quantitative mapping of groundwater depletion at the water management scale using a combined GRACE/InSAR approach. *Remote Sensing of Environment*, 205, pp.408-418. <https://doi.org/10.1016/j.rse.2017.11.025>

Castellazzi, P., Martel, R., Rivera, A., Huang, J., Pavlic, G., Calderhead, A.I., Chaussard, E., Garfias, J. and Salas, J., 2016. Groundwater depletion in Central Mexico: Use of GRACE and InSAR to support water resources management. *Water Resources Research*, 52(8), pp.5985-6003. <https://doi.org/10.1002/2015WR018211>

Charsley, T.J., Rathbone, P.A. and Lowe, D.J., 1990. *Nottingham: A geological background for planning and development*. British Geological Survey Technical Report, WA/90/1.

Chaussard, E., Bürgmann, R., Shirzaei, M., Fielding, E.J. and Baker, B., 2014. Predictability of hydraulic head changes and characterization of aquifer-system and fault properties from

InSAR-derived ground deformation. *Journal of Geophysical Research: Solid Earth*, 119(8), pp.6572-6590. <https://doi.org/10.1002/2014JB011266>

Chaussard, E., Milillo, P., Bürgmann, R., Perissin, D., Fielding, E.J. and Baker, B., 2017. Remote sensing of ground deformation for monitoring groundwater management practices: Application to the Santa Clara Valley during the 2012–2015 California drought. *Journal of Geophysical Research: Solid Earth*, 122(10), pp.8566-8582. <https://doi.org/10.1002/2017JB014676>

Chen, C.W. and Zebker, H.A., 2001. Two-dimensional phase unwrapping with use of statistical models for cost functions in nonlinear optimization. *JOSA A*, 18(2), pp.338-351. <https://doi.org/10.1364/JOSAA.18.000338>

Cigna, F. and Sowter, A., 2017. The relationship between intermittent coherence and precision of ISBAS InSAR ground motion velocities: ERS-1/2 case studies in the UK. *Remote Sensing of Environment*, 202, pp.177-198. <https://doi.org/10.1016/j.rse.2017.05.016>

Crosetto, M., Monserrat, O., Cuevas-González, M., Devanthéry, N. and Crippa, B., 2016. Persistent scatterer interferometry: A review. *ISPRS Journal of Photogrammetry and Remote Sensing*, 115, pp.78-89. <https://doi.org/10.1016/j.isprsjprs.2015.10.011>

Cuenca, M.C., Hooper, A.J. and Hanssen, R.F., 2013. Surface deformation induced by water influx in the abandoned coal mines in Limburg, The Netherlands observed by satellite radar interferometry. *Journal of Applied Geophysics*, 88, pp.1-11. <https://doi.org/10.1016/j.jappgeo.2012.10.003>

Donnelly, L.J., 2006. A review of coal mining induced fault reactivation in Great Britain. *Quarterly Journal of Engineering Geology and Hydrogeology*, 39(1), pp.5-50. <https://doi.org/10.1144/1470-9236/05-015>

Downing, R.A., Land, D.H., Allender, R., Lovelock, P.E.R., and Bridge, L.R., 1970. *The Hydrogeology of the Trent River Basin*. Hydrogeological Report, No. 5. Institute of Geological Sciences, London.

Duff, P., McL. D. 1992. Economic Geology. *In: Duff, P. McL. D, Smith, & AJ (eds). Geology of England and Wales*. The Geological Society, London, pp.599-637.

Dumpleton, S., Robins, N.S., Walker, J.A. and Merrin, P.D., 2001. Mine water rebound in South Nottinghamshire: risk evaluation using 3-D visualization and predictive modelling.

Quarterly Journal of Engineering Geology and Hydrogeology, 34(3), pp.307-319.

<https://doi.org/10.1144/qjegh.34.3.307>

Dumpleton, S., Glover, B.W., Butcher, A.S., Coleby, L.M. and Robins, N.S., 1995. *The impact of colliery closures on water resources, with particular regard to NRA Severn-Trent Region*. British Geological Survey Technical Report. WD/95/40.

European Environment Agency, 2012. *CORINE Land Cover 2012*. Available at:

<<https://land.copernicus.eu/pan-european/corine-land-cover/clc-2012/view>> [Accessed 25th August 2019].

Edwards, W.N., 1967. Geology of the country around Ollerton. (explanation of one-inch geological sheet 113, new series). Institute of Geological Sciences. HMSO, London. pp.297.

Farr, T.G., Rosen, P.A., Caro, E., Crippen, R., Duren, R., Hensley, S., Kobrick, M., Paller, M., Rodriguez, E., Roth, L. and Seal, D., 2007. The shuttle radar topography mission. *Reviews of geophysics*, 45(2). <https://doi.org/10.1029/2005RG000183>

Galloway, D.L. and Hoffmann, J., 2007. The application of satellite differential SAR interferometry-derived ground displacements in hydrogeology. *Hydrogeology Journal*, 15(1), pp.133-154. <https://doi.org/10.1007/s10040-006-0121-5>

Gammons, C.H., Duaine, T.E., Parker, S.R., Poulson, S.R. and Kennelly, P., 2010. Geochemistry and stable isotope investigation of acid mine drainage associated with abandoned coal mines in central Montana, USA. *Chemical Geology*, 269(1-2), pp.100-112. <https://doi.org/10.1016/j.chemgeo.2009.05.026>

Gee, D., Bateson, L., Sowter, A., Grebby, S., Novellino, A., Cigna, F., Marsh, S., Banton, C. and Wyatt, L., 2017. Ground motion in areas of abandoned mining: application of the Intermittent SBAS (ISBAS) to the Northumberland and Durham Coalfield, UK. *Geosciences*, 7(3), p.85. <https://doi.org/10.3390/geosciences7030085>

Gee, D., Sowter, A., Grebby, S., de Lange, G., Athab, A. and Marsh, S., 2019. National geohazards mapping in Europe: Interferometric analysis of the Netherlands. *Engineering Geology*, 256, pp.1-22. <https://doi.org/10.1016/j.enggeo.2019.02.020>

Gee, D., Sowter, A., Novellino, A., Marsh, S. and Gluyas, J., 2016. Monitoring land motion due to natural gas extraction: Validation of the Intermittent SBAS (ISBAS) DInSAR algorithm over gas fields of North Holland, the Netherlands. *Marine and Petroleum Geology*, 77, pp.1338-1354. <https://doi.org/10.1016/j.marpetgeo.2016.08.014>

Grebby, S., Orynassarova, E., Sowter, A., Gee, D. and Athab, A., 2019. Delineating ground deformation over the Tengiz oil field, Kazakhstan, using the Intermittent SBAS (ISBAS) DInSAR algorithm. *International Journal of Applied Earth Observation and Geoinformation*, 81, pp.37-46. <https://doi.org/10.1016/j.jag.2019.05.001>

- Guizar-Sicairos, M., Thurman, S.T. and Fienup, J.R., 2008. Efficient subpixel image registration algorithms. *Optics letters*, 33(2), pp.156-158. <https://doi.org/10.1364/OL.33.000156>
- Hanssen, R.F., Van Leijen, F.J., Van Zwieten, G.J., Dortland, S., Bremmer, C.N. and Kleuskens, M., 2008. Validation of PSI results of Alkmaar and Amsterdam within the TerraFirma validation project. In *Proceedings of FRINGE 2007* (pp. 26-30).
- Hiscock, K.M., 2009. *Hydrogeology: principles and practice*. John Wiley & Sons.
- Hoffmann, J., Zebker, H.A., Galloway, D.L. and Amelung, F., 2001. Seasonal subsidence and rebound in Las Vegas Valley, Nevada, observed by synthetic aperture radar interferometry. *Water Resources Research*, 37(6), pp.1551-1566. <https://doi.org/10.1029/2000WR900404>
- Holliday, D.W., 1986. Devonian and Carboniferous basins. In: Downing, R.A. and Gray, D.A. (eds) *Geothermal Energy: The Potential in the United Kingdom*. British Geological Survey, HMSO, London, 27, pp.84-109.
- Hulbert, A.G., and Terrington, R.L., 2014a. Metadata report for the East Midlands region of the Pennine Basin 1:250 000 resolution geological model. *British Geological Survey Open Report*, OR/14/026. 14pp.
- Hulbert, A.G., and Terrington, R.L., 2014b. Metadata report for the south-west Pennine Basin and adjacent area 1:250 000 resolution geological model. *British Geological Survey Open Report*, OR/14/027. 14pp.
- Jain, V.K., Dixit, M. and Chitra, R., 2015. Correlation of plasticity index and compression index of soil. *International Journal of Innovations in Engineering and Technology*, 5, pp.263-270.

Liu, P., Gao, Y., Shang, M. and Yi, X., 2020. Predicting water level rises and their effects on surrounding karst water in an abandoned mine in Shandong, China. *Environmental Earth Sciences*, 79(1), p.51. <https://doi.org/10.1007/s12665-019-8798-7>

Motagh, M., Shamshiri, R., Haghghi, M.H., Wetzel, H.U., Akbari, B., Nahavandchi, H., Roessner, S. and Arabi, S., 2017. Quantifying groundwater exploitation induced subsidence in the Rafsanjan plain, southeastern Iran, using InSAR time-series and in situ measurements. *Engineering geology*, 218, pp.134-151. <https://doi.org/10.1016/j.enggeo.2017.01.011>

Pearse, J., Singhroy, V., Samsonov, S. and Li, J., 2014. Anomalous surface heave induced by enhanced oil recovery in northern Alberta: InSAR observations and numerical modelling. *Journal of Geophysical Research: Solid Earth*, 119(8), pp.6630-6649. <https://doi.org/10.1002/2013JB010885>

Poland, J.F., 1984. *Guidebook to studies of land subsidence due to ground-water withdrawal*. UNESCO, Paris, France.

Rae, G.W., 1978. *Groundwater resources in the coalfields of England and Wales, B the Yorkshire Coalfield*. Technical Note. Central Water Planning Unit, Reading.

Rutqvist, J., Vasco, D.W. and Myer, L., 2010. Coupled reservoir-geomechanical analysis of CO₂ injection and ground deformations at In Salah, Algeria. *International Journal of Greenhouse Gas Control*, 4(2), pp.225-230. <https://doi.org/10.1016/j.ijggc.2009.10.017>

Sowter, A., Amat, M.B.C., Cigna, F., Marsh, S., Athab, A. and Alshammari, L., 2016. Mexico City land subsidence in 2014–2015 with Sentinel-1 IW TOPS: Results using the Intermittent SBAS (ISBAS) technique. *International Journal of Applied Earth Observation and Geoinformation*, 52, pp.230-242. <https://doi.org/10.1016/j.jag.2016.06.015>

Sowter, A., Athab, A., Novellino, A., Grebby, S. and Gee, D., 2018. Supporting energy regulation by monitoring land motion on a regional and national scale: A case study of Scotland. *Proceedings of the Institution of Mechanical Engineers, Part A: Journal of Power and Energy*, 232(1), pp.85-99. <https://doi.org/10.1177/0957650917737225>

Sowter, A., Bateson, L., Strange, P., Ambrose, K. and Syafiudin, M.F., 2013. DInSAR estimation of land motion using intermittent coherence with application to the South Derbyshire and Leicestershire coalfields. *Remote Sensing Letters*, 4(10), pp.979-987. <https://doi.org/10.1080/2150704X.2013.823673>

Terzaghi, K., 1925. Principles of soil mechanics, IV – Settlement and consolidation of clay. *Engineering News-Record*, 95(3), pp.874-878.

Van Tonder, G.J., Usher, B.H., Dennis, I. and Vermeulen, P.D., 2007. Predicting rebound in a deep colliery in South Africa. *Mine Water and the Environment*, 26(2), pp.79-87. <https://doi.org/10.1007/s10230-007-0154-6>

Wood, S.C., Younger, P.L. and Robins, N.S., 1999. Long-term changes in the quality of polluted mine water discharges from abandoned underground coal workings in Scotland. *Quarterly Journal of Engineering Geology and Hydrogeology*, 32(1), pp.69-79. <https://doi.org/10.1144/GSL.QJEG.1999.032.P1.05>

Wright, I.A., Paciuszkiewicz, K. and Belmer, N., 2018. Increased water pollution after closure of Australia's longest operating underground coal mine: A 13-month study of mine drainage, water chemistry and river ecology. *Water, Air, & Soil Pollution*, 229(3), p.55. <https://doi.org/10.1007/s11270-018-3718-0>

Wright, P. and Stow, R., 1999. Detecting mining subsidence from space. *International Journal of Remote Sensing*, 20(6), pp.1183-1188. <https://doi.org/10.1080/014311699212939>

Younger, P.L., 2016. A simple, low-cost approach to predicting the hydrogeological consequences of coalfield closure as a basis for best practice in long-term management. *International Journal of Coal Geology*, 164, pp.25-34. <https://doi.org/10.1016/j.coal.2016.06.002>

Younger, P.L. and Adams, R., 1999. *Predicting mine water rebound*. Environment Agency R&D Technical Report W179. Bristol, UK. 108pp.

Younger, P.L., 2002. Coalfield closure and the water environment in Europe. *Mining Technology*, 111(3), pp.201-209. <https://doi.org/10.1179/mnt.2002.111.3.201>

Younger, P.L., 1995. Mine water pollution in Britain: past, present and future. *Mineral planning*, 65, pp.38-41.